Maguire Andrew (Orcid ID: 0000-0002-6334-0497)
Griffin Kevin, Lee (Orcid ID: 0000-0003-4124-3757)
Schmiege Stephanie, C (Orcid ID: 0000-0001-9054-5538)

On the Functional Relationship Between Fluorescence and Photochemical Yields in Complex Evergreen Needleleaf Canopies

Andrew J. Maguire[1,2], Jan U.H. Eitel[1,2], Kevin L. Griffin[3,4], Troy S. Magney[5,6], Ryan A. Long[7], Lee A. Vierling[1,2], Stephanie C. Schmiege[4], Jyoti S. Jennewein[1], William A. Weygint[1,2] , Natalie T. Boelman[3], and Sarah G. Bruner[4]

[1]Department of Natural Resources and Society, University of Idaho, Moscow, ID, USA

[2]McCall Outdoor Science School, University of Idaho, McCall, ID, USA

[3]Department of Earth and Environmental Sciences, Lamont-Doherty Earth Observatory, Columbia University, New York, NY, USA

[4]Department of Ecology, Evolution and Environmental Biology, Columbia University, New York, NY, USA

[5]Department of Plant Sciences, University of California, Davis, CA, USA

[6]Division of Geological and Planetary Sciences, California Institute of Technology, Pasadena, CA, USA

[7]Department of Fish and Wildlife Sciences, University of Idaho, Moscow, ID 83844-1136, USA

Corresponding author: Andrew J. Maguire (amaguire@uidaho.edu)

Key Points:

- Needle-scale observations from forests show a nonlinear, irradiance-dependent relationship between fluorescence and photosystem II yields
- We use the breakpoint in this relationship to distinguish physiological constraints on photosystem II operating efficiency
- We use this relationship to contextualize the apparent linear relationship between fluorescence and carbon uptake at the canopy-scale

This article has been accepted for publication and undergone full peer review but has not been through the copyediting, typesetting, pagination and proofreading process which may lead to differences between this version and the Version of Record. Please cite this article as doi: 10.1029/2020GL087858

Abstract

Recent advancements in understanding remotely sensed solar-induced chlorophyll fluorescence often suggest a linear relationship with gross primary productivity at large spatial scales. However, the quantum yields of fluorescence and photochemistry are not linearly related and this relationship is largely driven by irradiance. This raises questions about the mechanistic basis of observed linearity from complex canopies that experience heterogeneous irradiance regimes at sub-canopy scales. We present empirical, data from two evergreen forest sites that demonstrate a nonlinear relationship between needle-scale observations of steady-state fluorescence yield and photochemical yield under ambient irradiance. We show that accounting for sub-canopy and diurnal patterns of irradiance can help identify the physiological constraints on needle-scale fluorescence at 70-80% accuracy. Our findings are placed in the context of how solar-induced chlorophyll fluorescence observations from spaceborne sensors relate to diurnal variation in canopy-scale physiology.

Plain Language Summary

Chlorophyll fluorescence is a faint signal emitted by plants that can provide information about photosynthesis and other processes important for plant growth. However, fluorescence is governed by complex chemical reactions that depend on light and it is not linearly related to photosynthetic carbon uptake. Ecosystems with complex canopy structure, such as evergreen needleleaf forests, experience dynamic sunlit and shaded conditions which make fluorescence observations challenging to interpret. However, by accounting for incoming light at fine spatial scales in studies using fluorescence, we can track the conditions under which canopies are partitioned by light-saturated and light-limited physiological constraints at 70-80% accuracy. Findings from our field-based study are relevant for interpreting satellite-based measurements of fluorescence as a proxy of photosynthetic carbon uptake. Furthermore, our study underscores the need for further research on how data from leaf-scale studies can be scaled up to shed light on ecosystem responses to changing climatic conditions.

1 Introduction

Advancements in measuring chlorophyll fluorescence (ChlF), particularly retrievals of solar-induced fluorescence (SIF) from satellite instruments, have led to improvements in understanding sensitivity of the terrestrial carbon cycle to environmental conditions (Guanter et al., 2014; Xing Li et al., 2018; Magney, Bowling, et al., 2019; Sun et al., 2017). Fluorescence is physically linked to the light reactions of photosynthesis (Alonso et al., 2017; Gu et al., 2019) and is sensitive to the quantity of light absorbed by foliage (i.e., absorbed photosynthetically active radiation, APAR) and to the efficiency which this light is used to drive photochemical processes (e.g., the quantum yield of photosystem II (Φ_{PSII}) and steady-state fluorescence yield (F_t)). SIF has proven useful for tracking seasonal dynamics of canopy physiology in evergreen needleleaf forests (ENFs) (Magney, Bowling, et al., 2019; Walther et al., 2016), for which traditional greenness indices – sensitive to turnover in leaf area and chlorophyll content – have limited value (Jeong et al., 2017). Yet, major uncertainties remain in deciphering the physiological constraints on Φ_{PSII} from SIF (Magney, Bowling, et al., 2019). Pulse amplitude modulated (PAM) fluorometry can be used to actively measure quantum yields (Baker, 2008) which remains challenging from passive SIF observations (Magney et al., 2017). Photochemistry is governed by intrinsic (e.g., genotypic) and extrinsic (e.g., nutrient availability; water, temperature, and radiation stress) controls (Baker, 2008; Krause & Weis, 1991; Maxwell & Johnson, 2000). However, over short-time scales two competing processes are primarily responsible for shaping the ChlF– Φ_{PSII} relationship. Under saturating irradiance, Φ_{PSII} is low and F_t is limited by nonphotochemical quenching

(NPQ-limited) – manifesting as dissipation of excess APAR as heat – which induces a positive relationship between Φ_{PSII} and F_t. Under non-saturating irradiance, NPQ is suppressed and F_t is limited by photochemical quenching (PQ-limited), which induces a negative relationship between Φ_{PSII} and F_t (Baker, 2008; Maxwell & Johnson, 2000; Porcar-Castell et al., 2014).

The complex canopy structure of ENFs leads to dynamic mosaics of highly illuminated and deeply shaded foliage at a sub-canopy scale, which in turn trigger within-canopy partitioning of NPQ and PQ, respectively. Remotely sensed data from ENFs thus represent an integration of the physiological responses to these aggregated irradiance conditions (Hilker, Coops, Hall, et al., 2008). Previous studies have demonstrated that high-resolution canopy structure measurements (e.g., from lidar) can help characterize heterogeneity in irradiance and constrain estimates of physiological responses at sub-canopy scales (Hall et al., 2008; Hilker et al., 2010; Hilker, Coops, Schwalm, et al., 2008; Middleton et al., 2009). Numerous studies have documented an apparent positive linear relationship between SIF and gross primary productivity (GPP) at canopy-to-landscape scales (Guanter et al., 2014; Xing Li et al., 2018; Sun et al., 2017), suggesting that NPQ is the dominant limitation. Prevalence of PQ-limitation has been linked to departures from linearity in the SIF—GPP relationship, especially in short-term studies that control for seasonal variation (Porcar-Castell et al., 2014; van der Tol et al., 2014; Wieneke et al., 2018). However, there is a lack of empirical evidence from field studies in ENFs that provide mechanistic support for integrated canopy-scale NPQ- and PQ-limitation.

Empirical evidence from a needle-scale field experiment revealed a nonlinear relationship between Φ_{PSII} and F_t (Porcar-Castell et al., 2008, 2014). Because of this nonlinearity, F_t cannot be interpreted as a direct proxy of photosynthetic light use efficiency (GPP/APAR) without additional information. Similarly, laboratory studies on *Gossypium* sp. (van der Tol et al., 2014) and *Acer palmatum* leaves (Magney et al., 2017) provided evidence that the sign of slope of the relationship between Φ_{PSII} and F_t is largely dependent on the intensity of irradiance. These findings encourage further investigation of the dynamics and drivers of this relationship in ENF foliage under ambient irradiance. The transferability of this relationship, including how it changes from leaf- to canopy-scales and the threshold at which this sign change occurs, must be determined empirically (Magney et al., 2017; Magney, Frankenberg, et al., 2019; Raczka et al., 2019; Wen et al., 2020). This is important for understanding the physiological differences between processes driven by the light reactions of photosynthesis (F_t, SIF, and Φ_{PSII}) and processes driven by the dark reactions of photosynthesis (GPP) (Damm et al., 2010; Frankenberg & Berry, 2018; Gu et al., 2019). Furthermore, whereas F_t and Φ_{PSII} are quantum yield terms, SIF and GPP are strongly linked by their common driver – APAR by chlorophyll. Therefore, interpreting SIF as a proxy of GPP requires accounting for APAR, which is challenging to quantify (Frankenberg & Berry, 2018) especially in complex canopies.

Because most current spaceborne SIF retrievals have fixed diurnal overpass times, studies reliant on such data cannot fully account for canopy irradiance dynamics. Mechanistically, it is likely that NPQ is the limiting factor in early afternoon spaceborne SIF retrievals (e.g., TROPOMI, OCO-2, and GOSAT), because the observations occur near peak diurnal irradiance when canopy self-shading is minimized. However, even if this is true, questions remain as to whether regularly timed ‘snapshots’ are representative of the physiological state of vegetation within the field of view (Magney, Frankenberg, et al., 2019; Parazoo et al., 2019). Research accounting for how variation in canopy illumination induces physiological regulation of photochemical processes has been limited to modeling studies (Celesti et al., 2018; van der Tol, Verhoef, & Rosema, 2009; van der Tol, Verhoef, Timmermans, et al., 2009) and controlled lab experiments (van der Tol et al., 2014).

Diurnally variable (e.g., OCO-3) (Eldering et al., 2019) and continuous (e.g., GeoCARB) (Moore III et al., 2018) observations of spaceborne SIF will provide an opportunity to investigate this effect at large-scales. First, however, it will be critical to leverage PAM fluorometry to understand the conditions under which the relationships among SIF, GPP, F_t, and Φ_{PSII} diverge.

We present empirical, field-based needle-scale observations of PAM ChlF from two shade-tolerant ENF species under ambient irradiance. We collected data over a constrained time period to minimize seasonal effects on Φ_{PSII} and F_t (e.g., changes in pigment content). We hypothesized that we would observe a nonlinear relationship between Φ_{PSII} and F_t, that the position of the breakpoint in this relationship (i.e., the threshold in Φ_{PSII} at which the relationship changes sign, signifying a transition between NPQ- and PQ-limitation) would converge with that of prior studies (Magney et al., 2017; Porcar-Castell et al., 2014; van der Tol et al., 2014) at $\Phi_{PSII} = 0.6$, and that the breakpoint would be driven by irradiance. To test these hypotheses we developed a simple model for predicting relative photochemical yield at a sub-canopy scale. We discuss whether this mechanistic model can aid interpretation of large-scale SIF observations from complex canopies experiencing dynamic shading regimes.

2 Materials and Methods

We implemented a novel experimental framework integrating observations of PAM ChlF with contemporaneous lidar-informed estimates of sub-canopy illumination regimes, the latter of which we validated with *in situ* observations. We then developed a simple model to predict relative Φ_{PSII} using F_t and irradiance.

2.1 Study sites

Field data were collected at two evergreen needleleaf sites: the forest-tundra ecotone near the Dalton Highway, Alaska, USA (67° 59′ 41″ N, 149° 45′ 16″ W, 730 m elevation; Eitel *et al*. 2019) on July 7-8, 2017 and a montane forest near McCall, Idaho, USA (44° 54′ 22″ N, 116° 4′ 0″ W, 1595 m elevation) on July 5-6, 2019. The Alaska site is dominated by white spruce (*Picea glauca*). The Idaho site has an understory of grand fir (*Abies grandis*) with an overstory of ponderosa pine (*Pinus ponderosa*) and Douglas fir (*Pseudotsuga menziesii*). Average daily temperature during sampling was 18.0° C and 17.0° C for the Alaska and Idaho sites, respectively. Average daily soil moisture during sampling was 0.24 m^3 m^{-3} and 0.11 m^3 m^{-3} at 10 cm depth for the Alaska and Idaho sites, respectively. Sites were not experiencing drought or disturbance during sampling. Sampling occurred during clear-sky conditions such that the canopies experienced a broad range of variability in sunlit-shading patterns across the day. Four groups of needles from outer branches at 1 – 2 m height above ground from each of 36 *P. glauca* study trees (*n* = 144) in Alaska and six groups of needles from each of 10 *A. grandis* study trees (*n* = 60) in Idaho were sampled. To observe a range of variability in illumination, sampling locations were distributed across crown aspects.

2.2 Needle-scale chlorophyll fluorescence measurements

We measured ChlF using an Optisci OS30p+, a PAM fluorometer employing a red actinic light (Opti-Sciences, Inc. Hudson, New Hampshire, USA) at a saturating light intensity of 3500 μmol m^{-2} s^{-1}. Sampled needles were marked to enable repeated measurement. Leaf clips used for ChlF measurements were removed between each measurement to allow for foliage to adapt to ambient light. *P. glauca* needles were sampled six times during daylight hours across the two sampling days; *A. grandis* needles were sampled six times during daylight hours on the first day and once again shortly after sunrise on the second day. The ratio of light-adapted variable to maximal fluorescence ($F_v`/F_m`$) represents photosystem II yield (Φ_{PSII}) (Genty et al., 1989). Observations of steady-state fluorescence yield (F_t) were normalized to $F_{t,max}$ following Magney et al. (2017). F_t can be interpreted as a yield because reported values are effectively normalized by the intensity and frequency of the modulating light from the fluorometer which was consistent across samples. These parameters are analogous to commonly derived parameters of SIF studies: SIF_{yield} (i.e., F_t) and photosynthetic light use efficiency (i.e., Φ_{PSII}, not accounting for dark reactions) (Porcar-Castell et al., 2014). We excluded observations when raw measurements were too low to interpret, which may have resulted from insufficient foliage in the instrument viewing window. The final dataset included 523 observations from the Alaska site (98% of recorded observations) and 417 observations from the Idaho site (99% of recorded observations).

2.3 Remote sensing data for modeling needle-scale irradiance

In 2011, airborne lidar data (8 points m^{-2}) were acquired over a 6 km x 1.5 km footprint (Hubbard et al., 2011), covering the extent of the *in situ* ChlF sampling locations in Alaska. We assumed that this lidar survey represented canopy structure at the time of ChlF sampling due to slow vegetation growth rates among high latitude spruce trees (Gamache & Payette, 2004).

Contemporaneous with field sampling in Idaho, terrestrial lidar data (> 1 point cm^{-2}; 0.1 mrad beam divergence) were collected for a 150 m x 150 m footprint covering ChlF sampling locations and surrounding vegetation that obscured direct solar exposure. Sampled needles were labeled such that coordinates could be visually determined at sub-centimeter precision from the resulting point cloud.

A digital canopy surface model (DSM) of the Alaska site was interpolated from the airborne lidar dataset and gridded at 0.5 m resolution using the R package ‘lidR’ (Roussel et al., 2017). A DSM of the Idaho site was interpolated from the terrestrial lidar dataset and gridded at 0.10 m resolution using the R package ‘akima’ (Akima et al., 2016).

Sampled trees at the Alaska site were identified using an individual tree detection algorithm implemented in the R package ‘rLiDAR’ (Silva et al., 2017) and validated with field measurements. DSM grid cells collocated with sampled needles were manually selected using canopy height value and directional location within tree crown boundaries. Due to the coarser spatial resolution of the Alaska DSM and the narrow-crowned trees at the forest-tundra ecotone, we were unable to identify unique grid cells corresponding to all sampled needles unambiguously. We limited the sample population to grid cells with canopy height value 1.0-3.0 m, as a reasonable approximation of sampling height, and grid cells that could be identified as exclusively corresponding to a given cardinal direction (e.g., sampling locations could not be assigned to unique grid cells for crowns composed of a two-by-two grid cell square). If multiple grid cells fit the aforementioned criteria for a given sampling location, each of these grid cells were selected and the average irradiance value (*see section 2.4*) was used. Following this approach, coordinates of 89 *P. glauca* sampling locations were approximated.

Sampled trees at the Idaho site were identified from labels affixed to tree boles visible in the terrestrial lidar point cloud. Coordinates of sampling locations were extracted by manually selecting terrestrial lidar returns at the fluorometer leaf clip in the point cloud. Coordinates of 60 *A. grandis* sampling locations were approximated.

2.4 Irradiance estimation

2.4.1 Modeled irradiance

We used the R package ‘insol’ (Corripio, 2003, 2015) to model instantaneous irradiance for sampling locations using the DSMs (see section 2.3), geographic location, and atmospheric and surface reflectance parameters, the latter of which were interpolated from satellite remote sensing datasets (Levelt et al., 2006; Mesinger et al., 2006). This approach enabled estimation of direct and diffuse solar irradiance through two steps: (1) top-of-canopy (TOC) direct and diffuse irradiance were calculated based on atmospheric conditions and solar geometry; (2) following previous work exploring light environment effects on spectral reflectance-based indicators of light use efficiency (Hall et al., 2008; Hilker et al., 2010, 2011; Hilker, Coops, Schwalm, et al., 2008; Li & Strahler, 1985), TOC direct irradiance was modulated by canopy surface, accounting for the surface aspect of individual DSM grid cells (based on neighborhood analysis) relative to the normal of the incident solar angle. Next, the DSM was used to simulate shadow casting based on solar geometry. Direct irradiance for grid cells classified as shaded was nullified. Non-zero direct irradiance values were added to TOC diffuse irradiance to yield modeled irradiance for each sampling location.

2.4.2 Observed irradiance

A handheld PYR solar radiation sensor and ProCheck real-time reader (METER, Inc., Pullman, WA) were used to measure irradiance at sampled *A. grandis* needles from the Idaho site, concurrent with ChlF measurement. The instrument measured incoming radiation across the 360 – 1120 nm spectrum, to accuracies within 1 W m^{-2}. *In situ* observations of irradiance were not collected at the Alaska site.

2.5 Statistical methods

We fit mixed-effects models in the ‘lme4’ package in R (Bates et al., 2018) that included irradiance as a fixed effect and sampled needles as a random effect to account for autocorrelation of multiple measurements obtained from the same needles. We used marginal R^2 values (Nakagawa & Schielzeth, 2013) to quantify the degree to which irradiance explained variance in F_t and Φ_{PSII}. To test our first hypothesis of nonlinearity in the relationship between F_t and Φ_{PSII}, we pooled ChlF observations across sampling periods within each study site and fit both linear regression models and generalized additive models (GAMs) to those data using the ‘mgcv’ package in R (Wood, 2019). We compared linear versus nonlinear model fits using adjusted R^2, Akaike Information Criterion (AIC), and Akaike weights (w_i) (Burnham & Anderson, 2002). We identified the breakpoint in the relationship between Φ_{PSII} and F_t by determining where the first derivative (i.e., slope) of the GAM equaled zero and the slope switched from positive to negative, based on evidence for this shape by Porcar-Castell et al. (2014) and van der Tol et al. (2014). We then used this breakpoint as a basis for determining the degree to which irradiance alone could be used to parse whether a given observation of F_t corresponded to relatively low Φ_{PSII} (hence NPQ-limited) or relatively high Φ_{PSII} (hence PQ-limited) using generalized linear models with a binomial error distribution.

3 Results and Discussion

3.1 Variance in Φ_{PSII} driven by irradiance, F_t by NPQ- and PQ-limitation

Ambient irradiance explained limited variation in F_t (marginal R^2 values were < 0.001 and 0.14 for Alaska and Idaho, respectively) whereas it explained considerably more variation in Φ_{PSII} (marginal R^2 values were 0.17 and 0.68 for Alaska and Idaho, respectively). In Idaho, modeled irradiance explained notably less variation in F_t and Φ_{PSII} relative to observed irradiance (marginal $R^2 < 0.01$ and 0.23, respectively). Gu et al. (2019) and van der Tol et al. (2014) presented similar evidence and suggested this disparity is due to photosynthesis saturating at high irradiance whereas absolute fluorescence continues to increase. Among sampled needles in Idaho, both Φ_{PSII} and F_t declined rapidly in response to increased irradiance, implying temporary amplification of NPQ (Porcar-Castell et al., 2006, 2008); such a response was not apparent among sampled needles from the Alaska site (***Fig.***

S1). Discrepancies between sites may be attributable to the means by which irradiance was quantified: in Alaska irradiance was modeled whereas in Idaho irradiance was observed. In Idaho, we showed a moderate linear fit between observed and modeled irradiance (slope = 0.51; intercept = 84.53 W m^{-2}; RMSE = 271.53 W m^{-2}; $r^2 = 0.11$; $p < 0.001$). Error may arise from DSM resolution and inability to account for transmittance through the canopy resulting in mischaracterization of shading at sampling locations (***Fig. S2***).

3.2 F_t and Φ_{PSII} are nonlinearly related, primarily controlled by irradiance

For both study sites, GAMs provided better fits than linear models (Alaska: adjusted $R^2 = 0.10$ and 0.08, AIC = -744.76 and -738.478, $w_i = 0.96$ and 0.04; Idaho: adjusted $R^2 = 0.20$ and 0.16, AIC = -710.83 and -693.08, $w_i > 0.99$ and < 0.01). The smoothed terms (GAMs) and coefficients (linear models) were significant for both sites ($p < 0.001$). The ratio of w_i values indicated that GAMs were 23.10 and 7171.71 times more likely to be the better fitting models of F_t against Φ_{PSII}. GAMs aligned with the relationships described by Magney et al. (2017), Porcar-Castell et al. (2008, 2014), and van der Tol et al. (2014) and revealed a positive-to-negative sign change in the proportionality of Φ_{PSII} and F_t (***Fig. 1***), supporting our first hypothesis. Despite the site and species differences GAMs from each site converged at their respective Φ_{PSII} breakpoints (Alaska *P. glauca* $\Phi_{PSII} = 0.744$; Idaho *A. grandis* $\Phi_{PSII} = 0.757$). This was a notable departure from findings of prior studies which show convergence at $\Phi_{PSII} = 0.60$ (Magney et al., 2017; Porcar-Castell et al., 2014; van der Tol et al., 2014). That we observed NPQ-limitation across a broader range of Φ_{PSII} relative to prior studies may be related to the shade-tolerance of our study species. Sampling in our study occurred over short timeframes; yet, foliar and whole-plant physiology both respond to seasonal changes in environmental conditions (e.g., nutrient availability, water and temperature stress, and photoperiod). Therefore, future studies should investigate whether the shape of this relationship and the location of the Φ_{PSII} breakpoint changes seasonally and across species and environmental conditions.

The observed nonlinear relationship between Φ_{PSII} and F_t demonstrates that parameters of ChlF cannot be interpreted as a direct proxy of photosynthetic status. Where a given observation falls on this curve is dependent on irradiance (***Fig. 2***), supporting our third hypothesis and revealing a pathway to discern relative photochemical yield.

3.3 Empirical support for (bias of) linear SIF—GPP observations

Binning observations of Φ_{PSII} and F_t by temporal sampling windows, including those closely aligned with current satellite overpass times (e.g., GOME-2 and SCHIAMACHY at 09:30 local solar time (LST); GOSAT-2, OCO-2, and TROPOMI at 13:30 LST; see colored boxes outlining select plots, ***Fig. 2***), provides field-based visual evidence for observed linearity between spaceborne ‘snapshots’ of SIF and GPP. However, pooling observations across sampling periods suggests that this linear relationship is not universal; rather, SIF retrievals represent aggregated illumination conditions and hence a composite of NPQ- and PQ-limitation that are biased toward top-of-canopy. Despite our evidence that PQ-limitation occurs during all sampling periods (***Fig. 2***) ‘snapshot’ observations often fail to document the decline in F_t at which this breakpoint occurs (van der Tol et al., 2014; Yang et al., 2015). This may be driven by the discrepancy in the range of Φ_{PSII} values associated with NPQ-limitation relative to that of PQ-limitation. Despite this compressed range of variability, 40% and 55% of observations from Alaska and Idaho, respectively, were PQ-limited. Therefore, current spaceborne SIF retrievals, biased toward top-of-canopy, have limited capacity to detect the nuances of sub-canopy responses.

Fortunately, the recently launched OCO-3 instrument follows a precessing orbit, enabling comparison of SIF dynamics across diurnal retrievals. OCO-3 takes up to 70 days to fully capture diurnal variation in SIF for a given location, meaning diurnal variation will be entangled with seasonal variation (Eldering et al., 2019). A forthcoming NASA mission, the geostationary GeoCARB, will further enhance the temporal sampling advancements of OCO-3 by enabling diurnal observation of SIF at very high temporal resolution (2-3 hours) (Moore III et al., 2018). GeoCARB will enable rapid assessment of how linearity in the SIF—GPP relationship might diverge on diurnal and seasonal time-scales.

3.4 Employing irradiance dependence to predict relative Φ_{PSII} from ChlF

We fit smoothed curves using the loess function in R (R Core Team, 2017) through irradiance data (displayed in ***Fig. 2***) binned at 0.05 intervals of Φ_{PSII} to approximate irradiance at the breakpoint in the F_t—Φ_{PSII} relationship (displayed in ***Fig. 1***). Irradiance at the breakpoint was greater at the Alaska site (*P. glauca*; mean: 368 W m^{-2}; 95% confidence interval 310 – 426 W m^{-2}) than at the Idaho site (*A. grandis*; mean: 104 W m^{-2}; 95% confidence interval 33 – 178 W m^{-2}), respectively (***Fig. 3***). This discrepancy may be related to the means of estimating irradiance or in differences in activation of reversible NPQ (Magney, Bowling, et al., 2019; Raczka et al., 2019).

We used generalized linear models informed by irradiance alone to predict whether a given ChlF observation fell on the NPQ-limited or PQ-limited side of the breakpoint. This approach correctly assigned 70% and 80% of the observations from Alaska and Idaho, respectively. This approach correctly classified observations from Alaska as NPQ-limited more frequently than PQ-limited (78% and 57%, respectively), whereas the opposite was true for Idaho (60% and 97%, respectively). Modeled irradiance from Idaho correctly classified observations as NPQ-limited and as PQ-limited (25% and 86%, respectively, for an overall accuracy of 59%) less frequently than observed irradiance. These findings underscore the challenge of accurately estimating irradiance from canopy structure-informed modeling and the need for more detailed approaches to model within-canopy irradiance for complex canopies. Furthermore, our analyses suggest that whereas shaded foliage is likely PQ-limited – as expected – photochemistry of sunlit foliage may be governed by factors beyond irradiance (e.g., leaf temperature, vapor pressure deficit, soil conditions), which in turn affect NPQ (Baker, 2008; Damm et al., 2010; Maxwell & Johnson, 2000; van der Tol et al., 2014).

3.5 Implications for remotely sensing Φ_{PSII} from SIF over complex canopies

Studies linking tower-based SIF observations with contemporaneous leaf-scale PAM fluorescence measurements show promise for remotely sensing canopy physiological status (Magney, Bowling, et al., 2019; Magney, Frankenberg, et al., 2019; Raczka et al., 2019). Mechanistically understanding ChlF across scales of time and space (Magney et al., 2017) and over structurally complex canopies remains a scientific frontier (Nichol et al., 2019). Our results provide field-based evidence to complement findings from remote sensing-based studies that physiological regulation is particularly important for interpreting SIF at the landscape-scale over ENFs (e.g., Walther et al., 2016). Fine-scale heterogeneity in canopy irradiance strongly drives ChlF (Frankenberg & Berry, 2018) and recent studies suggest that accounting for irradiance may improve SIF-based modelling of seasonal variation in sustained NPQ in ENFs (Parazoo et al., 2020; Raczka et al., 2019). We provide an approach to parameterize radiative transfer models (e.g., SCOPE) with information on leaf-level physiology to improve performance of SIF-based terrestrial biosphere models (Parazoo et al., 2020). To determine the generality of this relationship and its application to interpreting large-scale SIF observations, future studies should evaluate how the shapes of the F_t–Φ_{PSII} and SIF–GPP relationships change across ecologically meaningful scales (e.g., crown, canopy or landscape) and seasons and for different species. Furthermore, studies examining SIF should be mindful that, mechanistically, its linkage to photosynthesis is limited to the light reactions and APAR.

Our findings raise several important questions: (i) given the prominence of PQ-limited, low irradiance observations at the needle-scale, how common is this constraint at the canopy-scale?; (ii) when integrating ChlF emission (e.g., from spaceborne SIF retrievals) of a canopy subject to dynamic, variegated illumination, do equal-area sub-canopy fractions of PQ- or NPQ-limited foliage impose the same weight on the overall SIF yield signal?; and (iii) to what degree are the accuracy of TBMs affected by the propagation of error associated with failing to account for the composition of NPQ- and PQ-limitation in observed SIF?

Acknowledgments

This research was supported by NASA FINESST grant 80NSSC19K1341 to AJM, NASA ABoVE grant NNX15AT86A to JUHE, LAV, NTB, and KLG, and USDA McIntire-Stennis grant 1018044 to JUHE. We thank the Nokes family for granting us access to the Herald Nokes Family Experimental Forest. We also thank Carlos A. Silva for contributions in processing the airborne lidar data. Algorithms for interpolating DSMs were adapted from programs written by Heather E. Greaves (Greaves et al., 2015, 2016). We thank Johanna E. Jensen for valuable discussions through this project. Fluorescence and irradiance data used in this research may be accessed from the Oak Ridge National Laboratory Distributed Active Archive Center (Maguire et al., 2020).

References

Akima, H., Gebhardt, A., Petzold, T., & Maechler, M. (2016). Package “akima.” Retrieved from http://cran.r-project.org/package=akima

Alonso, L., Van Wittenberghe, S., Amorós-López, J., Vila-Francés, J., Gómez-Chova, L., & Moreno, J. (2017). Diurnal cycle relationships between passive fluorescence, PRI and NPQ of vegetation in a controlled stress experiment. *Remote Sensing*, *9*(8). https://doi.org/10.3390/rs9080770

Baker, N. R. (2008). Chlorophyll Fluorescence: A Probe of Photosynthesis In Vivo. *Annual Review of Plant Biology*, *59*(1), 89–113. https://doi.org/10.1146/annurev.arplant.59.032607.092759

Bates, D., Maechler, M., Bolker, B., Walker, S., Christensen, R. H. B., Singmann, H., et al. (2018). Package “lme4.” *R Topics Documented*. https://doi.org/10.2307/2533043>

Burnham, K. P., & Anderson, D. R. (2002). *Model Selection and Inference: A practical information-theoretic approach* (2nd ed.). New York: Springer-Verlag.

Celesti, M., van der Tol, C., Cogliati, S., Panigada, C., Yang, P., Pinto, F., et al. (2018). Exploring the physiological information of Sun-induced chlorophyll fluorescence through radiative transfer model inversion. *Remote Sensing of Environment*, *215*, 97–108. https://doi.org/10.1016/j.rse.2018.05.013

Corripio, J. G. (2003). Vectorial algebra algorithms for calculating terrain parameters from DEMs and solar radiation modelling in mountainous terrain. *International Journal of Geographical Information Science*, *17*(1), 1–23. https://doi.org/10.1080/713811744

Corripio, J. G. (2015). Package ‘insol.’

Damm, A., Elber, J., Erler, A., Gioli, B., Hamdi, K., Hutjes, R., et al. (2010). Remote sensing of sun-induced fluorescence to improve modeling of diurnal courses of gross primary production (GPP). *Global Change Biology*, *16*(1), 171–186. https://doi.org/10.1111/j.1365-2486.2009.01908.x

Eldering, A., Taylor, T. E., O’Dell, C. W., & Pavlick, R. (2019). The OCO-3 mission: measurement objectives and expected performance based on 1 year of simulated data. *Atmospheric Measurement Techniques*, *12*(4), 2341–2370. https://doi.org/10.5194/amt-12-2341-2019

Frankenberg, C., & Berry, J. (2018). Solar Induced Chlorophyll Fluorescence: Origins, Relation to Photosynthesis and Retrieval. In *Comprehensive Remote Sensing* (pp. 143–162). Elsevier. https://doi.org/10.1016/B978-0-12-409548-9.10632-3

Gamache, I., & Payette, S. (2004). Height Growth Response of Tree Line Black Spruce to Recent Climate Warming across the Forest-Tundra of Eastern Canada. *Journal of Ecology*, *92*(5), 835–845.

Genty, B., Briantais, J.-M., & Baker, N. R. (1989). The relationship between the quantum yield of photosynthetic electron transport and quenching of chlorophyll fluorescence. *Biochimica et Biophysica Acta (BBA) - General Subjects*, *990*(1), 87–92. https://doi.org/10.1016/S0304-4165(89)80016-9

Greaves, H. E., Vierling, L. A., Eitel, J. U. H., Boelman, N. T., Magney, T. S., Prager, C. M., & Griffin, K. L. (2015). Estimating aboveground biomass and leaf area of low-stature Arctic shrubs with terrestrial LiDAR. *Remote Sensing of Environment*, *164*, 26–35. https://doi.org/10.1016/j.rse.2015.02.023

Greaves, H. E., Vierling, L. A., Eitel, J. U. H., Boelman, N. T., Magney, T. S., Prager, C. M., & Griffin, K. L. (2016). High-resolution mapping of aboveground shrub biomass in Arctic tundra using airborne lidar and imagery. *Remote Sensing of Environment*, *184*, 361–373. https://doi.org/10.1016/j.rse.2016.07.026

Gu, L., Han, J., Wood, J. D., Chang, C. Y. Y., & Sun, Y. (2019). Sun-induced Chl fluorescence and its importance for biophysical modeling of photosynthesis based on light reactions. *New Phytologist*, *223*(3), 1179–1191. https://doi.org/10.1111/nph.15796

Guanter, L., Zhang, Y., Jung, M., Joiner, J., Voigt, M., Berry, J. A., et al. (2014). Global and time-resolved monitoring of crop photosynthesis with chlorophyll fluorescence. *Proceedings of the National Academy of Sciences*, *111*(14), E1327–E1333. https://doi.org/10.1073/pnas.1320008111

Hall, F. G., Hilker, T., Coops, N. C., Lyapustin, A., Huemmrich, K. F., Middleton, E., et al. (2008). Multi-angle remote sensing of forest light use efficiency by observing PRI variation with canopy shadow fraction. *Remote Sensing of Environment*, *112*(7), 3201–3211. https://doi.org/10.1016/j.rse.2008.03.015

Hilker, T., Coops, N. C., Schwalm, C. R., Jassal, R. S., Black, T. A., & Krishnan, P. (2008). Effects of mutual shading of tree crowns on prediction of photosynthetic light-use efficiency in a coastal Douglas-fir forest. *Tree Physiology*, *28*(6), 825–834. https://doi.org/10.1093/treephys/28.6.825

Hilker, T., Coops, N. C., Hall, F. G., Black, T. A., Wulder, M. a., Nesic, Z., & Krishnan, P. (2008). Separating physiologically and directionally induced changes in PRI using BRDF models. *Remote Sensing of Environment*, *112*(6), 2777–2788. https://doi.org/10.1016/j.rse.2008.01.011

Hilker, T., Hall, F. G., Coops, N. C., Lyapustin, A., Wang, Y., Nesic, Z., et al. (2010). Remote sensing of photosynthetic light-use efficiency across two forested biomes: Spatial scaling. *Remote Sensing of Environment*, *114*(12), 2863–2874. https://doi.org/10.1016/j.rse.2010.07.004

Hilker, T., Coops, N. C., Hall, F. G., Nichol, C. J., Lyapustin, A., Black, T. A., et al. (2011). Inferring terrestrial photosynthetic light use efficiency of temperate ecosystems from space. *Journal of Geophysical Research: Biogeosciences*, *116*(3), 1–11. https://doi.org/10.1029/2011JG001692

Hubbard, T. D., Koehler, R. D., & Combellick, R. A. (2011). High-resolution lidar data for Alaska infrastructure corridors. Alaska Division of Geological & Geophysical Surveys. https://doi.org/http://doi.org/10.14509/22722

Jeong, S. J., Schimel, D., Frankenberg, C., Drewry, D. T., Fisher, J. B., Verma, M., et al. (2017). Application of satellite solar-induced chlorophyll fluorescence to understanding large-scale variations in vegetation phenology and function over northern high latitude forests. *Remote Sensing of Environment*, *190*, 178–187. https://doi.org/10.1016/j.rse.2016.11.021

Krause, G. H., & Weis, E. (1991). Chlorophyll Fluorescence and Photosynthesis: The Basics. *Annual Review of Plant Physiology and Plant Molecular Biology*, *42*(1), 313–349. https://doi.org/10.1146/annurev.pp.42.060191.001525

Levelt, P. F., van den Oord, G. H. J., Dobber, M. R., Mälkki, A., Visser, H., de Vries, J., et al. (2006). The ozone monitoring instrument. *IEEE Transactions on Geoscience and Remote Sensing*, *44*(5), 1093–1101. Retrieved from http://ieeexplore.ieee.org/lpdocs/epic03/wrapper.htm?arnumber=1624601

Li, Xiaowen, & Strahler, A. H. (1985). Geometric-Optical Bidirectional Reflectance Modeling of a Conifer Forest Canopy. *IEEE Transactions on Geoscience and Remote Sensing*, *GE-24*(5), 705–721. https://doi.org/10.1109/TGRS.1986.289706

Li, Xing, Xiao, J., He, B., Altaf Arain, M., Beringer, J., Desai, A. R., et al. (2018). Solar-induced chlorophyll fluorescence is strongly correlated with terrestrial photosynthesis for a wide variety of biomes: First global analysis based on OCO-2 and flux tower observations. *Global Change Biology*, *24*(9), 3990–4008. https://doi.org/10.1111/gcb.14297

Magney, T. S., Frankenberg, C., Fisher, J. B., Sun, Y., North, G. B., Davis, T. S., et al. (2017). Connecting active to passive fluorescence with photosynthesis: a method for evaluating remote sensing measurements of Chl fluorescence. *New Phytologist*, *215*(4), 1594–1608. https://doi.org/10.1111/nph.14662

Magney, T. S., Frankenberg, C., Köhler, P., North, G., Davis, T. S., Dold, C., et al. (2019). Disentangling changes in the spectral shape of chlorophyll fluorescence: Implications for remote sensing of photosynthesis. *Journal of Geophysical Research: Biogeosciences*, 2019JG005029. https://doi.org/10.1029/2019JG005029

Magney, T. S., Bowling, D. R., Logan, B. A., Grossmann, K., Stutz, J., Blanken, P. D., et al. (2019). Mechanistic evidence for tracking the seasonality of photosynthesis with solar-induced fluorescence. *Proceedings of the National Academy of Sciences*, *116*(24), 11640–11645. https://doi.org/10.1073/pnas.1900278116

Maguire, A. J., Eitel, J. U. H., Griffin, K. L., Schmiege, S. C., Bruner, S. G., Boelman, N. T., & Weygint, W. A. (2020). Needle-level chlorophyll fluorescence and irradiance, AK and ID, 2017-2019. Oak Ridge, Tennessee, USA: ORNL DAAC. https://doi.org/https://doi.org/10.3334/ORNLDAAC/1785

Maxwell, K., & Johnson, G. N. (2000). Chlorophyll fluorescence -- a practical guide. *Journal of Experimental Botany*, *51*(345), 659–668. https://doi.org/10.1093/jexbot/51.345.659

Mesinger, F., DiMego, G., Kalnay, E., Mitchell, K., Shafran, P. C., Ebisuzaki, W., et al. (2006). North American Regional Reanalysis. *Bulletin of the American Meteorological Society*, *87*(3), 343–360. https://doi.org/10.1175/BAMS-87-3-343

Middleton, E. M., Cheng, Y. Ben, Hilker, T., Black, T. A., Krishnan, P., Coops, N. C., & Huemmrich, K. F. (2009). Linking foliage spectral responses to canopy-level ecosystem photosynthetic light-use efficiency at a douglas-fir forest in Canada. *Canadian Journal of Remote Sensing*, *35*(2), 166–188. https://doi.org/10.5589/m09-008

Moore III, B., Crowell, S. M. R., Rayner, P. J., Kumer, J., O'Dell, C. W., O'Brien, D., et al. (2018). The Potential of the Geostationary Carbon Cycle Observatory (GeoCarb) to Provide Multi-scale Constraints on the Carbon Cycle in the Americas. *Frontiers in Environmental Science*, *6*(OCT), 1–13. https://doi.org/10.3389/fenvs.2018.00109

Nakagawa, S., & Schielzeth, H. (2013). A general and simple method for obtaining R2 from generalized linear mixed-effects models. *Methods in Ecology and Evolution*, *4*(2), 133–142. https://doi.org/10.1111/j.2041-210x.2012.00261.x

Nichol, C. J., Drolet, G., Porcar-Castell, A., Wade, T., Sabater, N., Middleton, E. M., et al. (2019). Diurnal and Seasonal Solar Induced Chlorophyll Fluorescence and Photosynthesis in a Boreal Scots Pine Canopy. *Remote Sensing*, *11*(3), 273. https://doi.org/10.3390/rs11030273

Parazoo, N. C., Frankenberg, C., Köhler, P., Joiner, J., Yoshida, Y., Magney, T., et al. (2019). Towards a Harmonized Long-Term Spaceborne Record of Far-Red Solar-Induced Fluorescence. *Journal of Geophysical Research: Biogeosciences*, 2019JG005289. https://doi.org/10.1029/2019JG005289

Parazoo, N. C., Magney, T. S., Norton, A., Raczka, B., Bacour, C., Maignan, F., et al. (2020). Wide discrepancies in the magnitude and direction of modelled SIF in response to light conditions. *Biogeosciences*, (February), 1–42. https://doi.org/10.5194/bg-2019-508

Porcar-Castell, A., Bäck, J., Juurola, E., & Hari, P. (2006). Dynamics of the energy flow through photosystem II under changing light conditions: a model approach. *Functional Plant Biology*, *33*(3), 229. https://doi.org/10.1071/FP05133

Porcar-Castell, A., Pfündel, E., Korhonen, J. F. J., & Juurola, E. (2008). A new monitoring PAM fluorometer (MONI-PAM) to study the short- and long-term acclimation of photosystem II in field conditions. *Photosynthesis Research*, *96*(2), 173–179. https://doi.org/10.1007/s11120-008-9292-3

Porcar-Castell, A., Tyystjärvi, E., Atherton, J., van der Tol, C., Flexas, J., Pfündel, E. E., et al. (2014). Linking chlorophyll a fluorescence to photosynthesis for remote sensing applications: Mechanisms and challenges. *Journal of Experimental Botany*, *65*(15), 4065–4095. https://doi.org/10.1093/jxb/eru191

R Core Team. (2017). R: A language and environment for statistical computing. Vienna, Austria: R Foundation for Statistical Computing. Retrieved from https://www.r-project.org

Raczka, B., Porcar-Castell, A., Magney, T., Lee, J. E., Köhler, P., Frankenberg, C., et al. (2019). Sustained Nonphotochemical Quenching Shapes the Seasonal Pattern of Solar-Induced Fluorescence at a High-Elevation Evergreen Forest. *Journal of Geophysical Research: Biogeosciences*, *124*(7), 2005–2020. https://doi.org/10.1029/2018JG004883

Roussel, J.-R., Auty, D., De Boissieu, F., & Meador, A. S. (2017). Package 'lidR.'

Silva, C. A., Crookston, N. L., Hudak, A. T., Vierling, L. A., Klauberg, C., & Cardil, A. (2017). Package 'rLiDAR.'

Sun, Y., Frankenberg, C., Wood, J. D., Schimel, D. S., Jung, M., Guanter, L., et al. (2017). OCO-2 advances photosynthesis observation from space via solar-induced chlorophyll fluorescence. *Science*, *358*(6360), eaam5747. https://doi.org/10.1126/science.aam5747

van der Tol, C., Verhoef, W., & Rosema, A. (2009). A model for chlorophyll fluorescence and photosynthesis at leaf scale. *Agricultural and Forest Meteorology*, *149*(1), 96–105. https://doi.org/10.1016/j.agrformet.2008.07.007

van der Tol, C., Verhoef, W., Timmermans, J., Verhoef, A., & Su, Z. (2009). An integrated model of soil-canopy spectral radiances, photosynthesis, fluorescence, temperature and energy balance. *Biogeosciences*, *6*, 3109–3129. Retrieved from http://getitatduke.library.duke.edu/?&url_ver=Z39.88-2004&url_ctx_fmt=info:ofi/fmt:kev:mtx:ctx&rft_val_fmt=info:ofi/fmt:kev:mtx:journal&rft.atitle=An integrated model of soil-canopy spectral radiances%2C photosynthesis%2C fluorescence%2C temperature and e

van der Tol, C., Berry, J. A., Campbell, P. K. E., & Rascher, U. (2014). Models of fluorescence and photosynthesis for interpreting measurements of solar-induced chlorophyll fluorescence. *Journal of Geophysical Research: Biogeosciences*, *119*(12), 2312–2327. https://doi.org/10.1002/2014JG002713.We

Walther, S., Voigt, M., Thum, T., Gonsamo, A., Zhang, Y., Köhler, P., et al. (2016). Satellite chlorophyll fluorescence measurements reveal large-scale decoupling of photosynthesis and greenness dynamics in boreal evergreen forests. *Global Change Biology*, *22*(9), 2979–2996. https://doi.org/10.1111/gcb.13200

Wen, J., Köhler, P., Duveiller, G., Parazoo, N. C., Magney, T. S., Hooker, G., et al. (2020). A framework for harmonizing multiple satellite instruments to generate a long-term global high spatial-resolution solar-induced chlorophyll fluorescence (SIF). *Remote Sensing of Environment*, *239*(December 2019), 111644. https://doi.org/10.1016/j.rse.2020.111644

Wieneke, S., Burkart, A., Cendrero-Mateo, M. P., Julitta, T., Rossini, M., Schickling, A., et al. (2018). Linking photosynthesis and sun-induced fluorescence at sub-daily to seasonal scales. *Remote Sensing of Environment*, *219*(September), 247–258. https://doi.org/10.1016/j.rse.2018.10.019

Wood, S. N. (2019). Package “mgcv.”

Yang, X., Tang, J., Mustard, J. F., Lee, J.-E., Rossini, M., Joiner, J., et al. (2015). Solar-induced chlorophyll fluorescence that correlates with canopy photosynthesis on diurnal and seasonal scales in a temperate deciduous forest. *Geophysical Research Letters*, *42*(8), 2977–2987. https://doi.org/10.1002/2015GL063201

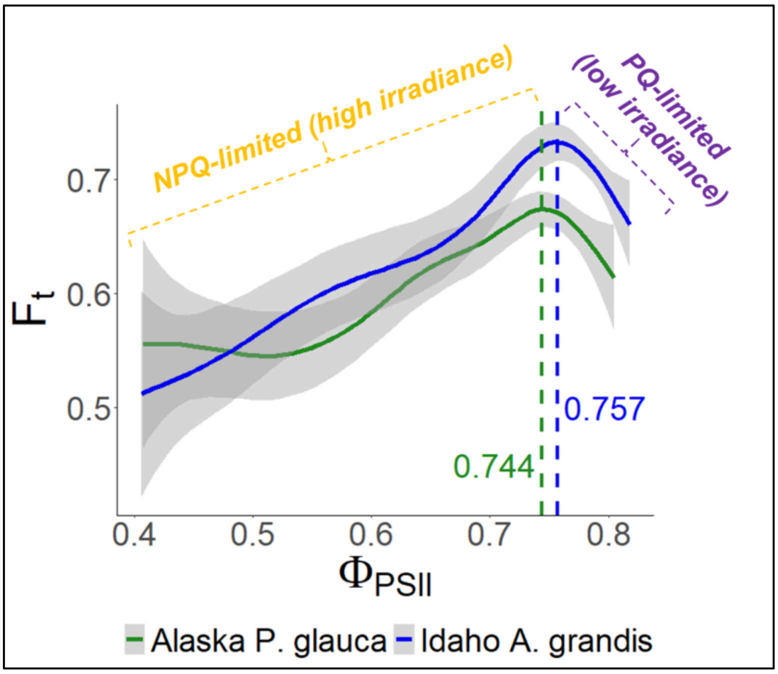

Figure 1. Generalized additive models (GAMs) fit to steady-state fluorescence yield (F_t) and photosystem II yield (Φ_{PSII}) for observations from Alaska *P. glauca* needles (green, *n* = 523) and Idaho *A. grandis* needles (blue, *n* = 417). 95% confidence intervals are show in gray. Breakpoints (dashed lines) were identified as the value of Φ_{PSII} at which the first derivative (i.e., slope) equaled zero and the slope switched from positive to negative. Observations of F_t were normalized to $F_{t,max}$ following Magney et al. (2017).

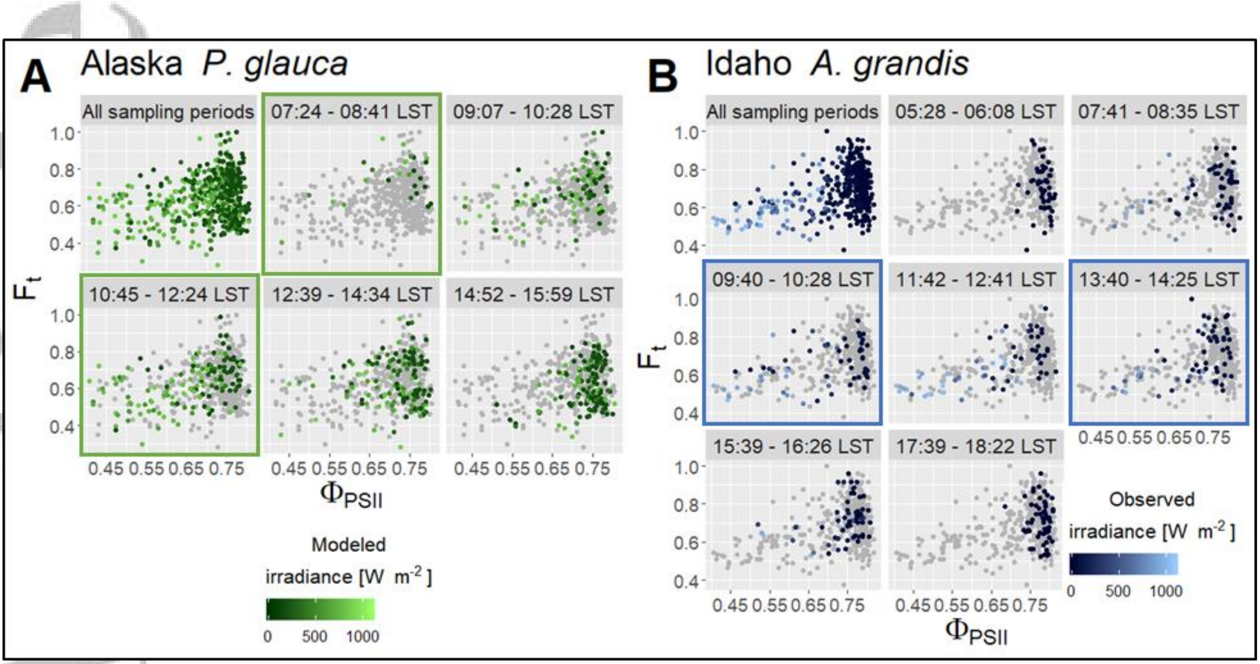

Figure 2. Relationship between steady-state fluorescence yield (F_t) and photosystem II yield (Φ_{PSII}) for *P. glauca* needles in Alaska (A; *n* = 523) and for *A. grandis* needles in Idaho (B; *n* = 417). Modeled (A) and observed (B) irradiance is indicated by coloration of points; grey points in individual sampling period panels (in local solar time, LST) show observations from other periods. Plots of sampling periods most closely aligned with timing of satellite overpasses (e.g., GOME-2 at 09:30 LST and TROPOMI at 13:30 LST) are outlined in colored boxes. Observations of F_t were normalized to $F_{t,max}$ following Magney et al. (2017).

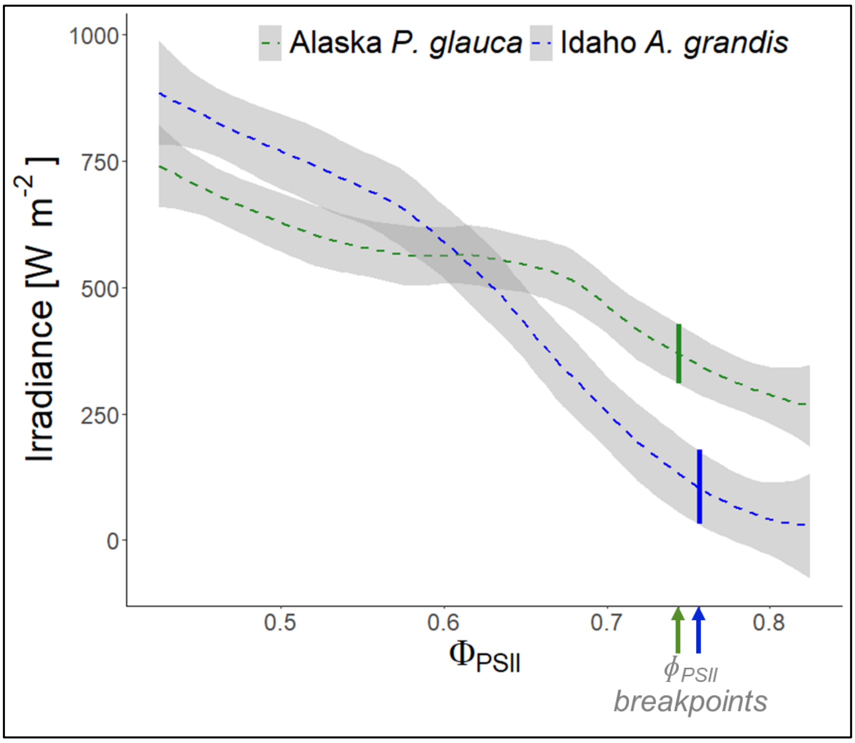

Figure 3. Distribution of modeled (Alaska *P. glauca*) and observed irradiance (Idaho *A. grandis*) by photosystem II yield (Φ_{PSII}) fit with smoothed curves and 95% confidence intervals using the loess function (R Core Team, 2017). Irradiance values are indicated associated with the respective breakpoints in fitted GAMs (see ***Fig. 1***).